# Fluid Dynamics from Causal-Budget Law

Dickson A Terrero

*Independent Researcher in Physics and Mathematics*

October 26, 2025

# Contents

## Abstract

We introduce a *causal-budget* formulation of fluid dynamics based on a single local principle: a finite, pointwise capacity for change. From kinetic theory (BGK/Maxwell), this yields a throughput constraint $|\mathbf{u}|^2 + v_{\text{int}}^2 \leq c^2$ relating parcel velocity to an internal transformation speed $v_{\text{int}} = (\nu\varepsilon)^{1/4} = \sqrt{\nu\,|S|}$, with capacity $c = \kappa a$ proportional to the sound speed $a = \sqrt{\gamma RT}$. Embedding this constraint in incompressible Navier–Stokes via a Lagrange multiplier produces a KKT system that admits a continuous energy inequality; a practical pointwise "causal projection" step yields a discrete energy decay and converges (subsequence) to a weak constrained solution in 2D. The framework recovers classical scalings – including the Kolmogorov dissipation length and near-wall viscous scaling – as equilibria of the causal budget, offering a unifying interpretation across inviscid, viscous, laminar, and turbulent regimes. Numerically, 1D channel and 2D lid-driven cavity tests enforce the constraint with 100% compliance and remain robust at high Reynolds numbers. Beyond a stability device, the formulation provides a diagnostic of *causal efficiency* (external vs. internal allocation) and a physics-grounded alternative to ad hoc closures, with clear microphysical calibration of $c$ and $v_{\text{int}}$.

# Part 1: Conceptual Foundation & Mathematical Translation

# 1   Define Core Fluid Concepts in Causal-Budget Terms

## 1.1 Internal Transformation in Fluids

We identify multiple forms of internal transformation in fluids (internal flow states):

- **Viscous dissipation rate ($\varepsilon$):** Primary mechanism for incompressible Newtonian fluids.

- **Temperature change/heat transfer:** For non-isothermal flows, includes conduction and convection.

- **Chemical reactions:** Species transformation with associated energy changes.

- **Phase changes:** Latent heat effects in multiphase flows.

- **Turbulent energy cascade:** Energy transfer between scales as internal reorganization (non-dissipative within the inertial range).

For a general fluid parcel, the total internal transformation power combines these effects.

## 1.2 Fluid Parcel Proper Time Definition

For a fluid parcel of mass $\delta m$, we define proper time following the causal-budget framework [14]:

$$\tau_{\text{fluid}} = \frac{E_{\text{fluid}}}{P_{\text{fluid}}} \tag{1}$$

Where:

- $E_{\text{fluid}} = \delta m \cdot e$ is the total energy of the parcel.

- $P_{\text{fluid}} = \delta m \cdot \dot{e}$ is the power (rate of energy transformation).

- Specific energy $e$ includes: kinetic + internal + potential components.

For a continuum fluid element at position $\mathbf{x}$:

$$\tau(\mathbf{x}, t) = \frac{e(\mathbf{x}, t)}{\dot{e}(\mathbf{x}, t)} \tag{2}$$

The material derivative gives the proper time evolution:

$$\frac{D\tau}{Dt} = \frac{D}{Dt}\left(\frac{e}{\dot{e}}\right) \tag{3}$$

## 1.3 Fluid Causal-Budget Law

The fundamental constraint for each fluid parcel (local causal capacity) [14]:

$$c^2 = |\mathbf{u}|^2 + v_{\text{int}}^2 \tag{4}$$

Where:

- $\mathbf{u}$ is the flow velocity (external motion).

- $v_{\text{int}}$ is the internal transformation rate (internal motion).

We define $v_{\text{int}}$ in measurable fluid terms, following the classical description of viscous dissipation [1, 4].

$$v_{\text{int}} = \sqrt{\nu \varepsilon} = \nu \sqrt{2 S_{ij} S_{ij}} \tag{5}$$

Alternative definitions for different transformation types:

$$v_{\text{int,thermal}} = \sqrt{\alpha \dot{T}} \qquad \text{(thermal transformation)} \tag{6}$$

$$v_{\text{int,chemical}} = \sqrt{D \dot{c}} \qquad \text{(species transformation)} \tag{7}$$

$$v_{\text{int,total}} = \sqrt{\sum_k v_{\text{int},k}^2} \qquad \text{(combined effect)} \tag{8}$$

# 2 Mathematical Formulation

## 2.1 Continuum Causal-Budget Formulation

Translate from discrete systems to continuum field theory [14]:

$$\mathcal{C}(\mathbf{x}, t) = \rho(\mathbf{x}, t)c^2 \quad \text{(causal capacity density)} \tag{9}$$

Local causal budget partition:

$$\rho c^2 = \rho|\mathbf{u}|^2 + \rho v_{\text{int}}^2 = \mathcal{K} + \mathcal{V}_{\text{int}} \tag{10}$$

Or in normalized density form:

$$1 = \frac{|\mathbf{u}|^2}{c^2} + \frac{v_{\text{int}}^2}{c^2} \tag{11}$$

Differential form of causal conservation (assuming $\rho c^2$ is conserved by bulk flow):

$$\frac{\partial}{\partial t}(\rho c^2) + \nabla \cdot (\rho c^2 \mathbf{u}) = 0 \tag{12}$$

## 2.2 Reformulate Navier-Stokes in Causal-Budget Variables

Start with the incompressible Navier–Stokes equations [1, 4]:

$$\frac{\partial u_i}{\partial t} + u_j \frac{\partial u_i}{\partial x_j} = -\frac{1}{\rho}\frac{\partial p}{\partial x_i} + \nu \nabla^2 u_i \tag{13}$$

$$\frac{\partial u_i}{\partial x_i} = 0 \tag{14}$$

Expressing in normalized form using $v_{\text{int}}$ (defined in the causal-budget law [14]), where $\nu \nabla^2 u_i$ is related to $v_{\text{int}}^2$ through the dissipation definition:

$$\frac{\partial}{\partial t}\left(\frac{u_i}{c}\right) + \frac{u_j}{c}\frac{\partial}{\partial x_j}\left(\frac{u_i}{c}\right) = -\frac{1}{\rho c^2}\frac{\partial p}{\partial x_i} + \frac{1}{2c}\nabla^2\left(\frac{v_{\text{int}}^2}{\nu}\right) \tag{15}$$

The non-linear term $\frac{u_j}{c}\frac{\partial}{\partial x_j}\left(\frac{u_i}{c}\right)$ appears as the convective causal transfer. Energy equation in causal-budget form:

$$\frac{D}{Dt}\left(\frac{1}{2}\frac{|\mathbf{u}|^2}{c^2} + \frac{v_{\text{int}}^2}{c^2}\right) = -\frac{1}{\rho c^2}\nabla \cdot (p\mathbf{u}) + \frac{\nu}{c^2}\nabla^2\left(\frac{1}{2}|\mathbf{u}|^2\right) - \frac{\varepsilon}{c^2} \tag{16}$$

## 2.3 Proper Time Transport Equation

From $\tau = e/\dot{e}$, derive evolution:

$$\frac{D\tau}{Dt} = \frac{1}{\dot{e}}\frac{De}{Dt} - \frac{e}{\dot{e}^2}\frac{D\dot{e}}{Dt} \tag{17}$$

For incompressible flow with viscous dissipation only, the specific total energy is $e = \frac{1}{2}|\mathbf{u}|^2$.

$$\frac{D\tau}{Dt} = \frac{\mathbf{u} \cdot \frac{D\mathbf{u}}{Dt}}{-\varepsilon} - \frac{\frac{1}{2}|\mathbf{u}|^2}{\varepsilon^2}\frac{D\varepsilon}{Dt} + \dots \quad \text{(including body forces/pressure work terms)} \tag{18}$$

## 2.4 Causal-Budget Constraint on Flow Evolution

The causal-budget law provides a constraint on possible flow states:

$$|\mathbf{u}(\mathbf{x}, t)| \leq c \quad \text{and} \quad v_{\text{int}}(\mathbf{x}, t) \leq c \tag{19}$$

This naturally bounds velocity and dissipation rates. The trade-off:

$$\text{High } |\mathbf{u}| \Rightarrow \text{Low } v_{\text{int}} \quad \text{and vice versa} \tag{20}$$

## 2.5 Dimensionless Groups in Causal-Budget Formulation

Natural dimensionless numbers emerge from the partition:

$$\text{Causal Reynolds number:} \quad \text{Re}_c = \frac{|\mathbf{u}|L}{\nu} \tag{21}$$

$$\text{Transformation number:} \quad \text{Tr} = \frac{v_{\text{int}}}{c} \tag{22}$$

$$\text{Causal Mach number:} \quad \text{Ma}_c = \frac{|\mathbf{u}|}{c} \tag{23}$$

The traditional Reynolds number is defined using a characteristic length scale $L$:

$$\text{Re} = \frac{|\mathbf{u}|L}{\nu} \tag{24}$$

# Part 2: Specific Fluid Applications

# 3  Boundary Layer Analysis

## 3.1 Near-Wall Causal Budget Partition

Consider a steady, incompressible boundary layer with streamwise velocity $u(y)$. The causal budget partition [14] becomes:

$$c^2 = u(y)^2 + v_{\text{int}}(y)^2 \tag{25}$$

Using $v_{\text{int}} = \sqrt{\nu\varepsilon}$ and $\varepsilon \approx \nu \left(\frac{du}{dy}\right)^2$ for simple shear:

$$v_{\text{int}}(y) \approx \nu \left|\frac{du}{dy}\right| \tag{26}$$

Thus the causal constraint becomes:

$$c^2 = u(y)^2 + \nu^2 \left(\frac{du}{dy}\right)^2 \tag{27}$$

## 3.2 Viscous Sublayer Prediction

In the viscous sublayer, $u(y) \approx \frac{u_\tau^2}{\nu}y$, where $u_\tau$ is friction velocity. The causal budget:

$$c^2 \approx \left(\frac{u_\tau^2}{\nu}y\right)^2 + \nu^2 \left(\frac{u_\tau^2}{\nu}\right)^2 = \frac{u_\tau^4}{\nu^2}y^2 + u_\tau^4 \tag{28}$$

The sublayer thickness variable $y^+ = \frac{u_\tau y}{\nu}$ can be determined by the point of causal equilibrium:

$$\text{Causal Equilibrium: } \frac{|\mathbf{u}|^2}{v_{\text{int}}^2} = 1 \Rightarrow \frac{(u_\tau^2 y/\nu)^2}{u_\tau^4} = 1 \Rightarrow y^+ = 1 \tag{29}$$

This predicts the causal equilibrium point occurs at $y^+ \approx 1$.

### 3.3 Trade-off Analysis in Boundary Layer

The velocity gradient enforces a trade-off consistent with the causal-budget limit [14]:

$$\frac{du}{dy} = \frac{\sqrt{c^2 - u(y)^2}}{\nu} \tag{30}$$

This suggests the maximum velocity gradient occurs at the wall where $u = 0$:

$$\left.\frac{du}{dy}\right|_{\text{wall}} = \frac{c}{\nu} \tag{31}$$

Which provides a physical bound on wall shear stress, $\tau_{\text{wall}} = \rho\nu\frac{c}{\nu} = \rho c$.

## 4 Turbulence Analysis

### 4.1 Causal Budget Across Scales

In the turbulent cascade [10, 11], different scales exhibit distinct causal-budget partitions [14]:

- **Large eddies (energy-containing range):**

$$|\mathbf{u}_L| \sim u_0, \quad v_{\text{int},L} \sim \sqrt{\nu\varepsilon_L} \ll |\mathbf{u}_L| \tag{32}$$

  High external motion, low internal transformation.

- **Inertial range eddies:**

$$|\mathbf{u}_\ell| \sim u_0 \left(\frac{\ell}{L}\right)^{1/3}, \quad v_{\text{int},\ell} \sim \sqrt{\nu\varepsilon} \cdot \left(\frac{\ell}{L}\right)^{-2/3} \tag{33}$$

  Balanced partition (reallocation of capacity occurs).

- **Dissipation range eddies:**

$$|\mathbf{u}_\eta| \sim u_0 \left(\frac{\eta}{L}\right)^{1/3}, \quad v_{\text{int},\eta} \sim \sqrt{\nu\varepsilon} \cdot \left(\frac{\eta}{L}\right)^{-2/3} \gg |\mathbf{u}_\eta| \tag{34}$$

  Low external motion, high internal transformation.

### 4.2 Richardson Cascade Through Causal Lens

The energy cascade can be viewed as a progressive reallocation of causal capacity:

$$\text{Large scales} \rightarrow \text{Intermediate scales} \rightarrow \text{Small scales} \tag{35}$$

$$\text{High } |\mathbf{u}|, \text{ Low } v_{\text{int}} \rightarrow \text{Balanced} \rightarrow \text{Low } |\mathbf{u}|, \text{ High } v_{\text{int}} \tag{36}$$

The cascade efficiency is constrained by the causal budget:

$$\frac{|\mathbf{u}_\ell|^2 + v_{\text{int},\ell}^2}{c^2} \le 1 \quad \text{for all scales } \ell \tag{37}$$

## 4.3 Kolmogorov Scales from Causal Principles

The Kolmogorov scale $\eta$ occurs when external and internal rates are comparable:

$$|\mathbf{u}_\eta| \sim v_{\text{int},\eta} \tag{38}$$

Using scaling laws for the inertial range, $|\mathbf{u}_\eta| \sim (\varepsilon\eta)^{1/3}$ and $v_{\text{int},\eta} \sim \sqrt{\nu\varepsilon}$, the equilibrium condition becomes:

$$(\varepsilon\eta)^{1/3} \sim \sqrt{\nu\varepsilon} \tag{39}$$

Solving for $\eta$ recovers the classical Kolmogorov scale:

$$\eta \sim \left(\frac{\nu^3}{\varepsilon}\right)^{1/4} \tag{40}$$

This recovers the classical Kolmogorov scale from causal-budget equilibrium.

## 4.4 Energy Transfer Mechanism

The energy transfer rate $\varepsilon$ between scales is constrained by the maximum causal velocity and integral length scale $L$:

$$\varepsilon \leq \frac{c^3}{L} \quad \text{(maximum causal throughput)} \tag{41}$$

This provides a fundamental bound on turbulent intensity.

# 5 Special Cases

## 5.1 Inviscid Flow Limit

As $\nu \to 0$ (Euler equations) [1, 4]:

$$v_{\text{int}} = \sqrt{\nu\varepsilon} \to 0 \tag{42}$$

The causal budget [14] becomes:

$$c^2 = |\mathbf{u}|^2 + 0 \Rightarrow |\mathbf{u}| = c \tag{43}$$

This suggests inviscid flow would tend toward the causal speed limit $c$ unless constrained by pressure gradients.

## 5.2 Stokes Flow (Low Reynolds Number)

For Re $\ll 1$, inertial effects are negligible [1, 13]:

$$|\mathbf{u}| \ll c \Rightarrow v_{\text{int}} \approx c \tag{44}$$

Nearly all causal capacity is allocated to internal transformation. The momentum equation simplifies to:

$$0 = -\frac{1}{\rho}\nabla p + \nu\nabla^2\mathbf{u} \tag{45}$$

And the causal constraint provides an estimate for the pressure-viscous balance [14]:

$$\nu|\nabla^2\mathbf{u}| \approx \frac{c}{\rho}|\nabla p| \tag{46}$$

## 5.3 High Reynolds Number Limit

For $\text{Re} \gg 1$ in the inertial range [11, 1]:

$$|\mathbf{u}_\ell| \gg v_{\text{int},\ell} \tag{47}$$

Most causal capacity goes to external motion. The cascade is efficient with minimal dissipation until the Kolmogorov scale.

## 5.4 Causal-Budget Reynolds Number

Define a new Reynolds number based on causal partition:

$$\text{Re}_c = \frac{|\mathbf{u}|^2}{v_{\text{int}}^2} = \frac{\text{External Causal Allocation}}{\text{Internal Causal Allocation}} \tag{48}$$

This provides a direct measure of the flow regime:

- $\text{Re}_c \ll 1$: Stokes flow (transformation-dominated)

- $\text{Re}_c \sim 1$: Transitional flow (balanced)

- $\text{Re}_c \gg 1$: Turbulent flow (motion-dominated)

# 6 Numerical Validation and Causal Compliance

To verify the causal-budget framework, we performed some simulations:

## 6.1 Poiseuille Flow and Lid-Driven Cavity

**(a) 1D Poiseuille Flow** The numerical solution matches the analytical parabolic velocity profile. The internal transformation field $v_{\text{int}}(y) = (\nu|\varepsilon|)^{1/4}$ reproduces the expected near-wall amplification and centerline decay. Causal usage [1, 4, 2, 14],

$$\frac{u^2 + v_{\text{int}}^2}{c^2} \leq 1,$$

was satisfied globally to numerical precision, confirming complete causal compliance. The proper-time profile $\tau(y) = E/P$ remained finite and smooth across the channel.

**(b) 2D Lid-Driven Cavity** A causal-enforced solver (grid $N = 80$, $c = 1$) was run for Reynolds numbers $\text{Re} = 10$–$1000$. Each simulation converged stably with adaptive damping $\gamma_{\text{adapt}} = 0.4$, maintaining a global time-step consistent with both convective and diffusive CFL limits.

**Empirical Results.**

| Re | Kinetic Energy | Dissipation | Efficiency | Max Usage | Violation (%) |
|------|---------------|-------------|------------|-----------|---------------|
| 10   | 0.0341        | 3.571       | 0.152      | 1.000     | 0.00          |
| 50   | 0.1627        | 3.235       | 0.646      | 1.000     | 0.00          |
| 100  | 0.2126        | 1.969       | 0.810      | 1.000     | 0.00          |
| 200  | 0.2397        | 0.824       | 0.910      | 1.000     | 0.00          |
| 500  | 0.2550        | 0.477       | 0.956      | 1.000     | 0.00          |
| 1000 | 0.2548        | 0.316       | 0.974      | 1.000     | 0.00          |

**Interpretation.** Causal efficiency increases monotonically with Reynolds number, indicating that more of the total causal capacity is allocated to external motion as inertial dominance grows. Dissipation decreases consistently, reflecting reduced internal transformation activity. All cases maintained 100% causal compliance, validating the local constraint

$$c^2 = |\mathbf{u}|^2 + v_{\text{int}}^2$$

throughout the domain.

Figure 1 shows the 1D causal partitions, and Figure 2 displays the 2D cavity causal fields (velocity magnitude, internal transformation, external/internal allocations, and total causal usage). Both confirm physically smooth partitions and exact enforcement of the causal bound.

These results demonstrate that the causal-budget framework not only reproduces classical flow behavior but also provides a stable, bounded formulation of fluid dynamics consistent with its physical energy limits.

## 6.2 Causally–Constrained Navier–Stokes Validation

We augment the Navier–Stokes equations with a local throughput constraint [14]

$$|\mathbf{u}|^2 + v_{\text{int}}^2 \le c^2, \qquad v_{\text{int}}^2 = \theta \, \nu \, |S|. \tag{49}$$

Discretely, this constraint is enforced by a *proximal projection* [6, 5, 7] – a velocity rescaling followed by Leray projection – that implements the KKT complementarity at the discrete level. The map is *nonexpansive in $L^2$* and therefore cannot increase kinetic energy within a projection step. Off the active set the solver recovers the standard Navier–Stokes evolution; on it, the causal cap introduces additional a priori bounds such as

$$|S| \le \frac{c^2}{\theta \, \nu}, \qquad \varepsilon \lesssim \frac{c^4}{\nu}. \tag{50}$$

**Kelvin–Helmholtz validation.** For a periodic shear layer ($N = 256$, $\text{Re} = 2 \times 10^4$), causal runs produce velocity spectra with fitted slopes $n \simeq -4.05$ to $-4.12$ (depending on $c$), systematically modifying the energy distribution while pruning high–$k$ content. **Crucially, the constraint remains substantially active across all tested capacities** (about 80–85% active–set fraction), indicating physical relevance rather than mere numerical regularization. Over the tested range the statistics show smooth trends with capacity: empirically,

$$E \sim c^{2.3}, \qquad Z \sim c^{2.1},$$

while remaining strictly bounded throughout the evolution.

The kinetic energy $E(t)$ shows the expected bounded growth with capacity, whereas the enstrophy $Z(t)$ is controlled but not strictly monotone – both consistent with the discrete proximal formulation. Notably, even at the nominal capacity $c = 1$ the framework maintains significant regularization (large active set, nonzero projection dissipation) while recovering the control spectral slope $n \approx -4.03$, demonstrating smooth mathematical consistency.

Representative results (Fig. 3, Fig. 4, Fig. 5) show coherent KH vortices, predictable spectral modification, and physically bounded energy/enstrophy – all consistent with causal–budget dynamics. The identification $c \approx \kappa \, a$ remains a *modeling hypothesis* for compressible extension.

## 6.3 Capacity sweep: $\kappa$ and active–set dynamics

To quantify how the causal–capacity constraint regulates high–speed shear, we performed compressible–layer runs at nominal Mach number $M_0 = 2.0$ (oppositely directed streams of $\pm 2a$) and $Re = 2 \times 10^4$ on a $200 \times 128$ grid. The sole control parameter was the capacity factor $\kappa$, with $c = \kappa a$ defining the local causal–throughput ceiling. All other numerical parameters (time integration, Riemann flux, causal projection step) were identical across runs.

For each case we record: (i) the active–set fraction $\phi$, representing the proportion of cells that violated the causal budget and were projected back to feasibility; (ii) the mean kinetic energy density removed by projection, $Q_{\text{mean}}^{\text{proj}}$; and (iii) the spatially averaged kinetic energy $E = \frac{1}{2}\langle |u|^2 \rangle$ after the first relaxation step ($t \approx 4 \times 10^{-2}$). Table 1 summarizes the results.

Table 1: Effect of $\kappa$ on projection activity and retained kinetic energy. Here $c = \kappa a$ is the local capacity speed, $\phi$ is the fraction of cells projected at $t=0$, $Q_{\text{mean}}^{\text{proj}}$ is the mean kinetic energy per unit volume removed at $t=0$, and $E$ is the kinetic energy at $t \approx 0.04$.

| Run ($\kappa$) | $c = \kappa a$ | $\phi$ @ $t=0$ (%) | $Q_{\text{mean}}^{\text{proj}}$ | $E$ @ $t \approx 0.04$ |
|---|---|---|---|---|
| 0.3 | $0.3\,a$ | 52.3 | 2.190 | 0.0257 |
| 0.4 | $0.4\,a$ | 50.7 | 2.172 | 0.0445 |
| 0.6 | $0.6\,a$ | 50.7 | 2.122 | 0.0952 |

The pattern is monotonic and robust:

(i) All three runs begin with $\phi \approx 0.5$, confirming that the initial $M_0=2$ layer is globally over–capacity and must be clipped.

(ii) The energy removal $Q_{\text{mean}}^{\text{proj}}$ decreases monotonically with $\kappa$. Smaller $\kappa$ implies a lower admissible capacity $c$, enforcing stronger kinetic–to–internal transfer at $t = 0$.

(iii) The surviving kinetic energy $E$ increases smoothly with $\kappa$. At $\kappa = 0.3$, nearly all macroscopic shear is erased; at $\kappa = 0.6$, a substantial fraction remains.

(iv) The temporal activity of the projector also varies: for $\kappa=0.3$ the active set persists over many timesteps ($\phi > 0$ beyond startup), indicating recurrent corrections of local shear; for $\kappa=0.6$ the projector switches off immediately after the first step ($\phi \rightarrow 0$), and the flow subsequently evolves by ordinary viscous decay with no further causal intervention.

Overall, $\kappa$ acts as a continuous *robustness–fidelity dial*. Low $\kappa$ yields maximum boundedness at the cost of strong energy removal, whereas high $\kappa$ preserves more kinetic energy and structure but provides a weaker guarantee against later over–capacity events. The transition between these regimes is smooth and can be tuned to achieve the desired stability margin for a given flow configuration.

## 6.4 Intrinsic dissipation timescale

For each run we define an operational dissipation timescale

$$\tau_K \equiv \frac{K}{\varepsilon_{\text{visc}} + \varepsilon_{\text{causal}}}, \qquad K = \tfrac{1}{2}\langle |u|^2 \rangle, \tag{51}$$

where $\varepsilon_{\text{visc}}$ is the physical viscous dissipation rate and $\varepsilon_{\text{causal}}$ is the causal–projection rate (proportional to $Q^{\text{proj}}_{\text{mean}}/\Delta t$ in the solver output). $\tau_K$ measures the characteristic time over which the present kinetic energy would be dissipated at the current combined rate.

In the strongly constrained case ($\kappa{=}0.3$), the persistent activity of the projector keeps $\varepsilon_{\text{causal}}$ finite, so $\tau_K$ remains small – energy is continuously consumed by capacity enforcement. For $\kappa{=}0.6$, the causal dissipation vanishes after the initial clip ($\varepsilon_{\text{causal}} \to 0$), and $\tau_K$ grows rapidly, indicating slow, nearly inviscid decay. The timescale thus provides a direct, diagnostic measure of how the causal–capacity law regulates the effective evolution rate of the flow.

## 6.5 Summary of Numerical Tests

Across all configurations, the causal–capacity formulation maintains complete compliance with the throughput constraint (49) while reproducing the expected physical behaviors of laminar and transitional flows. The causal projector acts as an adaptive stabilizer, locally removing excess kinetic energy only when the capacity limit is exceeded. The parameter $\kappa$ was shown to provide a quantitative handle on this regulation, with decreasing $\kappa$ enforcing stronger suppression of unstable shear and shorter effective dissipation timescales (§6.4). These results confirm that the causal–budget law yields a bounded yet tunable extension of Navier–Stokes dynamics – recovering classical flow structure in the high-$\kappa$ limit while ensuring robust stability under strong gradients.

### Outlook

Next steps include systematic $\theta$–parameter sweeps, dual–band spectral analysis for robustness, and extension of the present $\kappa$–sweep toward fully compressible regimes to refine the empirical relation $c = \kappa a$. Additional diagnostics such as the dissipation timescale $\tau_K$ (§6.4) will be incorporated to quantify how causal enforcement modifies the effective relaxation dynamics across different flow conditions.

# Part 3: Derivation From First-Principles

# 7    Model: Navier–Stokes Under a Causal-Capacity Constraint

Let $\Omega \subset \mathbb{R}^d$ ($d = 2, 3$) be a bounded domain, $t \in (0, T)$. Unknowns are velocity $\mathbf{u}(\mathbf{x}, t)$, pressure $p(\mathbf{x}, t)$, and a nonnegative Lagrange multiplier $\lambda(\mathbf{x}, t)$ that enforces a pointwise *causal-capacity* constraint [14]. Density $\rho > 0$, viscosity $\nu > 0$, body force $\mathbf{f}$, and capacity $c(\mathbf{x}, t) > 0$ are given.

**Internal rate and budget.**    Let

$$S(\mathbf{u}) = \tfrac{1}{2}\Big(\nabla\mathbf{u} + (\nabla\mathbf{u})^{\top}\Big), \qquad \varepsilon(\mathbf{u}) = 2\nu\, S(\mathbf{u}) : S(\mathbf{u}),$$

and define the internal "speed"

$$v_{\text{int}}(\mathbf{u}) = \big(\nu\,\varepsilon(\mathbf{u})\big)^{1/4} = \big(2\nu^2\, S(\mathbf{u}) : S(\mathbf{u})\big)^{1/4}.$$

The (pointwise) capacity constraint is

$$\phi(\mathbf{u}) \; := \; |\mathbf{u}|^2 + v_{\text{int}}(\mathbf{u})^2 - c^2 \; \leq 0 \qquad \text{a.e. in } \Omega \times (0, T). \tag{52}$$

## 7.1 Strong/KKT formulation

We seek $(\mathbf{u}, p, \lambda)$ satisfying [3, 6]

$$\rho\big(\partial_t \mathbf{u} + \mathbf{u} \cdot \nabla \mathbf{u}\big) = -\nabla p + \rho\nu\,\Delta\mathbf{u}\; -\; 2\lambda\,\mathbf{u}\; +\; \mathbf{f}, \qquad \text{in } \Omega \times (0,T), \tag{53}$$

$$\nabla \cdot \mathbf{u} = 0, \qquad \text{in } \Omega \times (0,T), \tag{54}$$

$$\phi(\mathbf{u}) \le 0, \quad \lambda \ge 0, \quad \lambda\,\phi(\mathbf{u}) = 0, \qquad \text{a.e. in } \Omega \times (0,T), \tag{55}$$

[1] with suitable initial and boundary conditions (e.g. no-slip $\mathbf{u}|_{\partial\Omega} = \mathbf{0}$, $\mathbf{u}(\cdot,0) = \mathbf{u}_0$). The extra term $-2\lambda\,\mathbf{u}$ is the calibrated opposing force generated by the capacity constraint and is active only on the *active set* $\mathcal{A}(t) = \{\mathbf{x} : |\mathbf{u}|^2 + v_{\text{int}}^2 = c^2\}$.

**Lemma 1** (Energy inequality). *Assume* $\mathbf{u}|_{\partial\Omega} = \mathbf{0}$. *Testing* (53) *with* $\mathbf{u}$ *yields*

$$\frac{\rho}{2}\frac{d}{dt}\|\mathbf{u}\|_{L^2(\Omega)}^2 + \rho\nu\,\|\nabla\mathbf{u}\|_{L^2(\Omega)}^2 + 2\int_\Omega \lambda\,|\mathbf{u}|^2\,dx = (\mathbf{f}, \mathbf{u})_{L^2(\Omega)}.$$

*In particular, the constraint is* dissipative*:* $\lambda \ge 0$ *can only remove kinetic energy.*

**Remark 1** (Coupling via lagged $v_{\text{int}}$). *Because* $v_{\text{int}}$ *depends on* $\nabla\mathbf{u}$, *the feasible set in* (52) *is nonconvex in* $\mathbf{u}$. *For analysis and robust numerics one may* lag *the internal rate, replacing* $v_{\text{int}}(\mathbf{u})$ *by a known* $v_{\text{int}}^\sharp$ *built from the previous time level/iterate. This convexifies the local constraint and leads to a variational inequality with a convex, time-dependent obstacle.*

## 7.2 Weak (variational-inequality) form

Let

$$V = \{\mathbf{v} \in H_0^1(\Omega)^d \,:\, \nabla \cdot \mathbf{v} = 0\}, \qquad a(\mathbf{u}, \mathbf{v}) = \rho\nu \int_\Omega \nabla\mathbf{u} : \nabla\mathbf{v}\,dx.$$

With $v_{\text{int}}^\sharp$ given (Remark 1), define the convex set

$$K(t) = \left\{ \mathbf{v} \in V \,:\, |\mathbf{v}(\mathbf{x})|^2 \le c(\mathbf{x},t)^2 - \big(v_{\text{int}}^\sharp(\mathbf{x},t)\big)^2 \;\text{ a.e. } \right\}.$$

**Problem (VI).** Find $\mathbf{u}(t) \in K(t)$ such that, for all $\mathbf{w} \in K(t)$,

$$\langle \rho\,\partial_t \mathbf{u}, \mathbf{w} - \mathbf{u} \rangle + a(\mathbf{u}, \mathbf{w} - \mathbf{u}) + \rho \int_\Omega (\mathbf{u} \cdot \nabla)\mathbf{u} \cdot (\mathbf{w} - \mathbf{u})\,dx \;\ge\; (\mathbf{f}, \mathbf{w} - \mathbf{u}). \tag{56}$$

Standard results on Navier–Stokes variational inequalities with obstacles [4, 5] imply existence of weak solutions; the multiplier $\lambda$ is a nonnegative measure supported on the active set and recovers the KKT system (53)–(55).

## 7.3 Time-discrete projection scheme (capacity step)

Given $(\mathbf{u}^n, p^n)$ at time $t^n$, a practical scheme proceeds as:

**(S1) Tentative NS step** The tentative velocity $\boldsymbol{u}^*$ (and $p^{n+1}$) are obtained by any incompressible Navier–Stokes integrator, e.g. [2],

$$\frac{\rho}{\Delta t}\big(\boldsymbol{u}^* - \boldsymbol{u}^n\big) + \rho\,(\boldsymbol{u}^n \cdot \nabla)\boldsymbol{u}^* = -\nabla p^{n+1} + \rho\nu\,\Delta\boldsymbol{u}^* + \boldsymbol{f}^{n+1},$$

$$\nabla \cdot \boldsymbol{u}^* = 0.$$

13

**(S2) Build lagged internal rate** Set $v_{\text{int}}^{\sharp} = (\nu \, \varepsilon(\mathbf{u}^*))^{1/4}$ (optionally clamp $v_{\text{int}}^{\sharp} \leq c$).

**(S3) Pointwise capacity projection** For each $\mathbf{x} \in \Omega$, project $\mathbf{u}^*(\mathbf{x})$ onto the local convex set $K^{\sharp}(\mathbf{x}) = \{\mathbf{v} : |\mathbf{v}|^2 \leq c^2 - (v_{\text{int}}^{\sharp})^2\}$.

$$
\mathbf{u}^{n+1}(\mathbf{x}) = \begin{cases} \mathbf{u}^*(\mathbf{x}), & |\mathbf{u}^*|^2 \leq c^2 - (v_{\text{int}}^{\sharp})^2, \\[2mm] \mathbf{u}^*(\mathbf{x}) \sqrt{\dfrac{c^2 - (v_{\text{int}}^{\sharp})^2}{|\mathbf{u}^*(\mathbf{x})|^2}}, & \text{otherwise.} \end{cases} \tag{57}
$$

This is the solution of the proximal subproblem $\min_{\mathbf{v}} \frac{1}{2}\|\mathbf{v} - \mathbf{u}^*\|^2$ s.t. $|\mathbf{v}|^2 \leq c^2 - (v_{\text{int}}^{\sharp})^2$.

**(S4) Discrete multiplier (diagnostic)** On the active set of (57), the KKT condition $\mathbf{u}^{n+1} - \mathbf{u}^* + 2\lambda^{n+1}\mathbf{u}^{n+1} = 0$ gives

$$
\lambda^{n+1}(\mathbf{x}) = \frac{1}{2}\left(\frac{|\mathbf{u}^*(\mathbf{x})|}{|\mathbf{u}^{n+1}(\mathbf{x})|} - 1\right) = \frac{1}{2}\left(\sqrt{\frac{|\mathbf{u}^*(\mathbf{x})|^2}{c^2 - (v_{\text{int}}^{\sharp})^2}} - 1\right) \geq 0, \tag{58}
$$

and $\lambda^{n+1} = 0$ elsewhere. (If the proximal is weighted by $\rho/\Delta t$, multiply the right-hand side by $\rho/\Delta t$.) The capacity step adds *only* dissipative work, consistent with Lemma 1.

**Remark 2** (Consistency with the implemented solver). *The streamfunction–vorticity update plus your adaptive damping and internal clamping can be read as performing (S1) with an explicit transport step, building $v_{\text{int}}^{\sharp}$ from the tentative field, and then applying the pointwise projection (57). Reporting with the* clamped $v_{\text{int}}$ *aligns with the KKT feasibility $\phi(\mathbf{u}^{n+1}) \leq 0$.*

# 8  Energy inequality, existence, and calibration of the capacity $c$

Throughout this section we adopt the internal rate used in the numerics [1]:

$$
v_{\text{int}}(\mathbf{u}) := \big(\nu \, \varepsilon(\mathbf{u})\big)^{1/4}, \qquad \varepsilon(\mathbf{u}) = 2\nu \, S(\mathbf{u}) : S(\mathbf{u}), \quad S(\mathbf{u}) = \tfrac{1}{2}(\nabla\mathbf{u} + \nabla\mathbf{u}^{\top}).
$$

The pointwise capacity constraint is

$$
|\mathbf{u}|^2 + v_{\text{int}}(\mathbf{u})^2 \; \leq \; c^2 \quad \text{a.e. in } \Omega \times (0, T).
$$

When the constraint is active, a nonnegative Lagrange multiplier $\lambda$ appears in the momentum balance:

$$
\rho(\partial_t\mathbf{u} + \mathbf{u}\cdot\nabla\mathbf{u}) = -\nabla p + \rho\nu \, \Delta\mathbf{u} - 2\lambda \, \mathbf{u} + \mathbf{f},
$$
$$
\lambda \geq 0, \quad \lambda\big(|\mathbf{u}|^2 + v_{\text{int}}^2 - c^2\big) = 0, \quad \nabla\cdot\mathbf{u} = 0. \tag{59}
$$

with no-slip boundary conditions [3, 6].

**Continuous energy inequality**

**Theorem 1** (Energy inequality). *Let $(\mathbf{u}, p, \lambda)$ satisfy (59) in the weak sense, with $\mathbf{u} \in L^{\infty}(0, T; L^2_{\sigma}(\Omega)) \cap L^2(0, T; H^1_0(\Omega)^d)$, $\mathbf{f} \in L^2(0, T; H^{-1})$, and no-slip walls. Then*

$$
\frac{\rho}{2}\frac{d}{dt}\|\mathbf{u}(t)\|_{L^2}^2 + \rho\nu\|\nabla\mathbf{u}(t)\|_{L^2}^2 + 2\int_{\Omega} \lambda(\mathbf{x}, t)\,|\mathbf{u}|^2\, dx \; \leq \; \langle\mathbf{f}, \mathbf{u}\rangle_{H^{-1}, H^1_0},
$$

$$
a.e. \; t \in (0, T).
$$

*In particular, the multiplier term is* dissipative, *so the constrained dynamics enjoys at least as much energy decay as standard NSE.*

**Remark 3.** *Testing* (59) *with* $\mathbf{u}$, *using* $\nabla \cdot \mathbf{u} = 0$ *and no-slip, makes the convection and pressure work vanish;* $-2\lambda \mathbf{u} \cdot \mathbf{u} \leq 0$ *provides the extra damping channel.*

**Existence with lagged internal rate (convex feasible set)** Define at time level $t^{n+1}$ a *lagged* internal rate $v_{\text{int}}^{\sharp}$ from the previous iterate/time step and the convex set

$$K^{\sharp} := \left\{ \mathbf{v} \in H_0^1(\Omega)^d : \ \nabla \cdot \mathbf{v} = 0, \ \ |\mathbf{v}(\mathbf{x})|^2 \leq c^2 - \left(v_{\text{int}}^{\sharp}(\mathbf{x})\right)^2 \ \text{a.e.} \right\}.$$

**Theorem 2** (Existence, lagged obstacle). *Given* $\mathbf{u}_0 \in L_{\sigma}^2(\Omega)$, $\mathbf{f} \in L^2(0, T; H^{-1})$, *and a partition* $0 = t^0 < \cdots < t^N = T$, *the implicit Euler discretization of NSE on each slab, followed by the pointwise projection* $\mathbf{u}^{n+1} = \Pi_{K^{\sharp}}(\mathbf{u}^*)$ *of the tentative velocity* $\mathbf{u}^*$ *onto* $K^{\sharp}$, *admits a solution sequence bounded in* $\dots$ $L^{\infty}(0, T; L^2) \cap L^2(0, T; H_0^1)$. *As* $\Delta t \to 0$, *a subsequence converges (Aubin–Lions)* [7] *to a weak solution of* (59) *with the lagged constraint and satisfies the energy inequality above.*

*Proof sketch.* The feasible set $K^{\sharp}$ is closed and convex; the projection $\Pi_{K^{\sharp}}$ is nonexpansive in $L^2$. Energy stability of the implicit step plus nonexpansiveness of the projection gives uniform a priori bounds; compactness and the monotonicity of the normal cone to $K^{\sharp}$ yield a limit $(\mathbf{u}, p, \lambda)$.

**Discrete energy decay for the algorithm used in the paper** Let $\mathbf{u}^*$ be the velocity after the implicit Navier–Stokes step (with forcing), and set

$$\mathbf{u}^{n+1}(\mathbf{x}) = \begin{cases} \mathbf{u}^*(\mathbf{x}), & |\mathbf{u}^*(\mathbf{x})|^2 + (v_{\text{int}}^{\sharp})^2 \leq c^2, \\ \sqrt{\dfrac{c^2 - (v_{\text{int}}^{\sharp})^2}{|\mathbf{u}^*(\mathbf{x})|^2}} \, \mathbf{u}^*(\mathbf{x}), & \text{otherwise.} \end{cases}$$

**Lemma 2** (One-step decay). *With the update above,*

$$\frac{\rho}{2\Delta t}\left(\|\mathbf{u}^{n+1}\|_{L^2}^2 - \|\mathbf{u}^n\|_{L^2}^2\right) + \rho\nu\|\nabla\mathbf{u}^{n+1}\|_{L^2}^2 + \frac{\rho}{\Delta t}\int_{\Omega} \lambda^{n+1}|\mathbf{u}^{n+1}|^2 \, dx$$
$$\leq \ \langle \mathbf{f}^{n+1}, \mathbf{u}^{n+1} \rangle,$$

*where* $\lambda^{n+1} \geq 0$ *is the KKT multiplier of the pointwise projection. Hence the projection cannot increase kinetic energy; it only removes excess beyond capacity.*

*Proof sketch.* The implicit NSE step is energy stable; the projection is the $L^2$-closest feasible velocity (a proximal map to the indicator of $K^{\sharp}$), thus nonexpansive and dissipative [6].

**Remark on the fully coupled constraint** If the internal rate is not lagged, $K(\mathbf{u})$ depends on $\mathbf{u}$. On each time slab, the map $\mathbf{u} \mapsto \Pi_{K(\mathbf{u})}(\mathbf{u}^*)$ is compact and continuous under mild regularity; a Schauder fixed-point then gives existence for small time steps [3]. Details can be placed in an appendix.

**How to choose $c$: microphysics vs nondimensional capacity**

**Microphysical calibration** The bound $v_{\text{int}} \le c$ is equivalent to a *maximum dissipation rate per mass*

$$\varepsilon \ \le \ \varepsilon_{\max} := \frac{c^4}{\nu}.$$

For *simple shear* with $\varepsilon \approx \nu \, \dot\gamma^2$,

$$v_{\text{int}} = (\nu^2 \dot\gamma^2)^{1/4} = (\nu\dot\gamma)^{1/2}, \quad \Rightarrow \quad \dot\gamma_{\max} = \frac{c^2}{\nu}.$$

Thus measured thresholds for $\varepsilon$ or $\dot\gamma$ determine $c$. For compressible media one may tie $c$ to a fraction of the sound speed $a$ to forbid super-acoustic internal rates [13].

**Nondimensional capacity (the choice used numerically)** Pick $U_0, L_0$ and define $\hat{\mathbf{u}} = \mathbf{u}/U_0$, $\hat\nu = \nu/(U_0 L_0) = 1/\text{Re}$, $\hat c = c/U_0$. Then

$$\frac{|\hat{\mathbf{u}}|^2}{\hat c^2} + \frac{\hat v_{\text{int}}^2}{\hat c^2} \le 1, \qquad \hat v_{\text{int}} = (\hat\nu \, \hat\varepsilon)^{1/4}.$$

Choosing $U_0 = c$ gives $\hat c = 1$ and the constraint $|\hat{\mathbf{u}}|^2 + \hat v_{\text{int}}^2 \le 1$, which is exactly the normalization used in our solver and plots.

**Remark 4** (Physical meaning of $\lambda$). *The multiplier $\lambda$ acts as a calibrated opposing force that activates only when the local capacity is saturated; it extracts kinetic energy and converts it to internal transformation consistent with the constraint [14]. This is the continuum realization of the "energy vs. opposing calibrated force" principle.*

# 9 Microphysical derivations for $v_{\text{int}}$ and $c$

## 9.1 Internal transformation speed from kinetic theory

For a Newtonian fluid, $\mathbf{\Pi}' = 2\mu \, \mathbf{S}$ with $\mu = \rho\nu$ and $\mathbf{S} = \frac{1}{2}(\nabla\mathbf{u} + \nabla\mathbf{u}^\top)$ [1]. The viscous dissipation per unit mass is

$$\varepsilon \ = \ \frac{1}{\rho}\mathbf{\Pi}' : \nabla\mathbf{u} \ = \ 2\nu \, \mathbf{S} : \mathbf{S}, \qquad |S| := \sqrt{2\,\mathbf{S} : \mathbf{S}}.$$

We define the internal transformation speed by

$$\boxed{v_{\text{int}} \ := \ (\nu \, \varepsilon)^{1/4}}$$

and the following equivalent forms hold (Frobenius norm $\|\cdot\|_F$):

$$v_{\text{int}}^2 \ = \ (\nu\varepsilon)^{1/2} \ = \ \nu \, |S| \ = \ \frac{1}{\sqrt{2}} \frac{\|\mathbf{\Pi}'\|_F}{\rho}.$$

This is exactly the law used in the numerics; different tensor norms only change the $\mathcal{O}(1)$ prefactor.

## 9.2 Capacity speed from microphysics

Two independent microscopic bounds give $c = \mathcal{O}(a)$ where $a = \sqrt{\gamma RT}$ is the sound speed [13].

**(A) BGK relaxation/entropy–production bound.** In BGK, $f$ relaxes to $f^{\mathrm{eq}}$ on a time $\tau$, and linear transport gives $\mu = p\tau$, hence $\nu = \mu/\rho = (p/\rho)\,\tau = RT\,\tau$ [8]. The largest irreversible power per unit mass cannot exceed a fraction of the thermal energy over a relaxation time,

$$\varepsilon_{\max} \;\lesssim\; \beta\,\frac{e_{\mathrm{th}}}{\tau}, \qquad e_{\mathrm{th}} = c_v T = \frac{RT}{\gamma - 1}, \qquad \beta = \mathcal{O}(1). \tag{60}$$

Imposing $v_{\mathrm{int}} \le c$ via $v_{\mathrm{int}}^4 = \alpha\nu\varepsilon$ yields

$$c^4 = \alpha\,\nu\,\varepsilon_{\max} = \alpha(RT\,\tau)\,\frac{\beta RT}{(\gamma - 1)\tau} = \frac{\alpha\beta}{\gamma - 1}(RT)^2, \tag{61}$$

$$\boxed{\begin{array}{l} c = \left(\dfrac{\alpha\beta}{\gamma-1}\right)^{1/4}\sqrt{RT} = \kappa\,a, \\[2mm] \kappa = \left(\dfrac{\alpha\beta}{\gamma(\gamma-1)}\right)^{1/4} = \mathcal{O}(1) \end{array}} \tag{62}$$

**(B) Grad positivity/realizability bound.** Realizability of moments implies $\|\mathbf{\Pi}'\| \lesssim \chi\,p$ with $\chi = \mathcal{O}(1)$ [3]. Using $v_{\mathrm{int}}^2 = \|\mathbf{\Pi}'\|/\rho$ gives

$$v_{\mathrm{int}}^2 \;\le\; \frac{\chi p}{\rho} \;=\; \chi RT \;\Rightarrow\; \boxed{c \,\sim\, \sqrt{\chi RT} \;=\; \sqrt{\tfrac{\chi}{\gamma}}\,a.} \tag{63}$$

**Practical calibration.** In dimensional runs pick $c = \kappa a(T_0)$ with $\kappa \in [0.7, 1.0]$; in nondimensional runs set $c_{\mathrm{nd}} = 1$ and interpret it as fixing $U_0 = \kappa a$.

## 9.3 Implications

From $v_{\mathrm{int}} \le c$ one obtains a dissipation cap

$$\varepsilon \;\le\; \frac{c^4}{\alpha\,\nu} \;=\; \frac{\kappa^4\,\gamma^2 R^2 T^2}{\alpha\,\nu}, \tag{64}$$

and the local throughput constraint

$$\boxed{\frac{|\mathbf{u}|^2}{c^2} + \frac{v_{\mathrm{int}}^2}{c^2} \;\le\; 1} \tag{65}$$

which our numerical projection enforces pointwise.

**Theorem 3** (Kinetic-to-Macro Capacity Bound from BGK). *Let $f(t, x, v)$ solve the BGK model*

$$\partial_t f + v \cdot \nabla_x f \;=\; \frac{1}{\tau}\left(M[\rho, u, T] - f\right),$$

*with Maxwellian $M$ having macroscopic fields $(\rho, u, T)$ and relaxation time $\tau > 0$. Assume a near-equilibrium (small Knudsen) regime with finite fourth moments and a uniform relative-entropy bound $H(f|M) \le C_H$. Let $\mu = p\tau$ be the BGK viscosity, $\nu = \mu/\rho$ the kinematic viscosity, and $S = \frac{1}{2}(\nabla u + (\nabla u)^\top)$ the strain rate, with $|S| = \sqrt{2\,S{:}S}$.*
 *Define the internal transformation speed*

$$v_{\mathrm{int}} \;:=\; (\nu\,\varepsilon)^{1/4} \quad \text{with} \quad \varepsilon \;=\; 2\,\nu\,S{:}S.$$

*Then* $v_{\text{int}} = \sqrt{\nu\,|S|}$, *and there exist constants* $0 < \kappa \leq 1$ *and* $\theta \sim 1$ *(depending on Knudsen number, dimension, and* $\Pr$*) such that*

$$|u|^2 \;+\; v_{\text{int}}^2 \;\leq\; c^2 \;+\; \mathcal{O}(\mathrm{Kn}^2), \qquad c \;=\; \kappa\,a, \quad a = \sqrt{\gamma R T}.$$

*Equivalently, after nondimensionalization by* $u_* = a$ *one has the unit capacity bound* $|u|^2 + v_{\text{int}}^2 \leq 1 + \mathcal{O}(\mathrm{Kn}^2)$.

*Proof sketch.* (i) Chapman–Enskog to first order gives the Navier–Stokes closure and $\mu = p\tau$, hence $\varepsilon = 2\nu S{:}S$. Then $(\nu\varepsilon)^{1/4} = (2\nu^2 S{:}S)^{1/4} = \sqrt{\nu\,|S|}$.

(ii) Write $f = M + g$, with $g$ the non-equilibrium part. Relative-entropy bounds control moments of $g$ and imply a uniform bound on the deviatoric stress $\Pi = \int (v-u)\otimes(v-u)g\,dv$ in terms of $p$ and $a$. In the hydrodynamic limit ($\mathrm{Kn} \to 0$), this yields a pointwise inequality $|u|^2 + \theta\,\nu\,|S| \leq \kappa^2 a^2 + \mathcal{O}(\mathrm{Kn}^2)$ for some $0 < \kappa \leq 1$, $\theta \sim 1$. (iii) Substitute $v_{\text{int}}^2 = \nu|S|$ to obtain the stated form. $\qquad\square$

**Remark 5.** *The constant* $c = \kappa a$ *has a clear microphysical meaning: it is a fraction of the local sound speed determined by kinetic (finite-moment / finite-relaxation) bounds. In fully nondimensional variables using* $u_* = a$*, one simply has* $c \equiv 1$.

**Definition 1** (Causal-budget constrained NSE)**.** *Let* $\Omega \subset \mathbb{R}^d$ *be smooth. Define*

$$G(u, \nabla u) = |u|^2 + \nu\,|S(u)|_\delta - c^2, \qquad S(u) = \tfrac{1}{2}(\nabla u + \nabla u^\top), \quad |S|_\delta = \sqrt{2\,S{:}S + \delta^2}.$$

*We seek* $(u, p, \lambda)$ *with* $\lambda \geq 0$ *such that* [3, 6]

$$\partial_t u + (u \cdot \nabla)u + \nabla p - \nu \Delta u \;+\; 2\lambda\,u \;-\; \nabla\!\cdot\!\left(\lambda\,\frac{\nu}{2}\,\frac{S(u)}{|S(u)|_\delta}\right) \;=\; 0, \tag{66}$$

$$\nabla \cdot u = 0, \qquad G \leq 0, \qquad \lambda\,G = 0. \tag{67}$$

**Proposition 1** (Energy inequality)**.** *Assume no-slip on* $\partial\Omega$ *and define* $E(t) = \tfrac{1}{2}\|u(t)\|_{L^2(\Omega)}^2$ [4]. *Any sufficiently regular solution of* (66)–(67) *satisfies*

$$E(t) \;+\; \nu \int_0^t \|\nabla u\|_{L^2}^2\,ds \;+\; \int_0^t\!\!\int_\Omega \lambda\,u \cdot \partial_u G\,dx\,ds \;\leq\; E(0).$$

*In particular, the KKT term is nonnegative (dissipative) when active, so the constraint cannot create energy.*

*Proof sketch.* Take the $L^2$ inner product of (66) with $u$, integrate over $\Omega$. Convective and pressure terms vanish by incompressibility and boundary conditions. Viscous term yields $-\nu\|\nabla u\|_2^2$. Complementarity ensures $\lambda \geq 0$ and that on the active set $G = 0$, giving $u \cdot \partial_u G = 2|u|^2 \geq 0$. Hence the KKT contribution is nonnegative. $\qquad\square$

**Proposition 2** (Discrete energy inequality and multiplier recovery)**.** *Let* $E^n = \tfrac{1}{2}\|u^n\|_2^2$. *Suppose the advance operator* $\mathcal{A}_{\Delta t}$ *is energy stable:* $E(\tilde{u}^{n+1}) \leq E^n$. *Then the projection is nonexpansive in* $L^2$*:* $E^{n+1} \leq E(\tilde{u}^{n+1})$*, hence*

$$E^{n+1} \;\leq\; E^n \qquad \text{for all time steps.}$$

*Moreover, at any overshoot cell, the projection satisfies the KKT conditions of the pointwise problem* $\min_w \tfrac{1}{2}|w - \tilde{u}^{n+1}|^2$ *s.t.* $|w|^2 + v_{\text{int}}^2 \leq c^2$*, and the discrete multiplier is*

$$\lambda^{n+1}(x) \;=\; \frac{1 - s(x)}{s(x)}\,\frac{1}{\Delta t}, \qquad s(x) = \sqrt{\frac{(c^2 - v_{\text{int}}^2)_+}{|\tilde{u}^{n+1}|^2}}.$$

**Advance + Causal Projection**  Given $u^n$ divergence-free, compute a provisional step (any energy-stable NSE integrator)

$$\tilde{u}^{n+1} = \mathcal{A}_{\Delta t}(u^n),$$

then form $v_{\text{int}}^{n+1}$ from $\tilde{u}^{n+1}$ via $v_{\text{int}}^2 = \nu |S(\tilde{u}^{n+1})|$. Define the pointwise feasible ball $B_c(x) = \{w : |w|^2 + v_{\text{int}}^2(x) \le c^2\}$. Project $\tilde{u}^{n+1}$ onto $B_c$:

$$u^{n+1}(x) = \begin{cases} \tilde{u}^{n+1}(x), & |\tilde{u}^{n+1}|^2 + v_{\text{int}}^2 \le c^2, \\ s(x)\,\tilde{u}^{n+1}(x), \quad s(x) = \sqrt{\dfrac{(c^2 - v_{\text{int}}^2)_+}{|\tilde{u}^{n+1}|^2}}, & \text{otherwise.} \end{cases}$$

*Proof sketch.*  The projection is the Euclidean projection onto a closed convex set, hence a contraction in $L^2$ [6]. The KKT conditions for the pointwise quadratic program give $u^{n+1} = \tilde{u}^{n+1}/(1+\mu)$ with $\mu \ge 0$ chosen to make the constraint tight; identify $s = 1/(1+\mu)$ and set $\lambda = \mu/\Delta t$.  □

## 10   Discussion and Future Work

The numerical results confirm that the causal–capacity constraint $|\mathbf{u}|^2 + v_{\text{int}}^2 \le c^2$ provides a robust and physically interpretable mechanism for stabilizing high-speed and transitional flows [2, 1]. The projector acts as an adaptive energy regulator [5, 4] that enforces local throughput compliance without introducing spurious diffusion. By varying the parameter $\kappa$, the framework exposes a continuous spectrum between strict causal enforcement [14] (high dissipation, full stability) and nearly inviscid behavior (low dissipation, free evolution). This establishes a controllable connection between numerical stability and physical consistency.

Future extensions will focus on several directions: (i) extending the causal projector to compressible regimes with strong shocks [13], (ii) coupling with energy-based turbulence closures [11] that use the internal rate $v_{\text{int}}^2 = \theta_\mu \nu |S|$ as a subgrid measure, (iii) performing three–dimensional validation under sustained forcing to test convergence of the dissipation spectrum [10, 11], and (iv) examining wall-bounded and rotating systems where causal capacity interacts with boundary-layer detachment. Additional diagnostics such as the dissipation timescale $\tau_K = K/\varepsilon_{\text{visc+proj}}$ will enable quantitative comparison with classical turbulence scaling and serve as calibration observables for practical flow-control implementations.

## 11   Conclusion

We have introduced a causally–constrained extension of the Navier–Stokes equations in which the total kinetic and internal transformation rates are bounded by a finite capacity $c = \kappa a$ [13]. This constraint yields a mathematically closed and physically consistent flow evolution law that preserves the local energy inequality [4] while ensuring that the dynamics remain subcausal at all times [14]. The resulting projector–based solver demonstrates that the causal–budget law can stabilize supersonic and transitional flows without empirical tuning [5, 2, 14]. Across all tested configurations, energy removal occurs only where the constraint is active [3, 6], confirming that the method enforces stability through physical throughput limitation rather than artificial dissipation [4]. The capacity parameter $\kappa$ thus defines a tunable link between drag and stability [14], providing a systematic route to flow regulation that remains compatible with the governing conservation laws.

In summary, the causal–budget law offers a physically grounded, computationally stable alternative to standard regularization schemes [2, 5]. It unifies energy conservation, dissipation control, and causal compliance under a single operational principle that can be extended to broader classes of physical systems where finite transformation capacity governs evolution [14].

# Appendix

## A    Maxwell (BGK) Stress Relaxation and the Causal Capacity

A linearized BGK closure around equilibrium yields [8], for the deviatoric stress $\sigma$, the Maxwell (Oldroyd-A with zero retardation) model [1]

$$\tau_R \overset{\triangledown}{\sigma} + \sigma = 2\mu\, S, \qquad \mu = p\,\tau, \qquad \nu = \mu/\rho,$$

where $\overset{\triangledown}{\sigma}$ is the upper-convected derivative (reduce to material derivative in small-strain), and $\tau_R \sim \tau$ is the microscopic stress-relaxation time [3].

Define the elastic storage (per unit mass) $e_{\mathrm{int}} = \frac{1}{4G\rho}\, \sigma : \sigma$ with $G = \mu/\tau_R$ the shear modulus. The power input to the internal mode is $\sigma : S$ and the dissipation rate is $\phi = (1/2\mu)\, \sigma : \sigma$. A Cauchy–Schwarz estimate gives

$$\sigma : S \ \le\ 2\sqrt{G\rho\, e_{\mathrm{int}}}\ |S|.$$

Uniform $H$-theorem / moment bounds for BGK imply [8] $e_{\mathrm{int}} \le C_T\, a^2$ with $a = \sqrt{\gamma R T}$ and dimensionless $C_T = \mathcal{O}(1)$ in the hydrodynamic regime. Hence

$$\sigma : S \ \le\ C\, a\, |S|, \qquad C = \mathcal{O}(1).$$

On the other hand, the Navier–Stokes dissipation is $\varepsilon = 2\nu\, S : S$ and therefore

$$v_{\mathrm{int}} \ := \ (\nu\varepsilon)^{1/4} \ = \ \sqrt{\nu\, |S|}.$$

Combining the two estimates shows that the total "throughput" of external plus internal channels is bounded by a microphysical speed proportional to $a$ [13]:

$$|u|^2 + v_{\mathrm{int}}^2 \ \le\ (\kappa\, a)^2 \ + \ \mathcal{O}(\mathrm{Kn}^2),$$

for some $\kappa \in (0, 1]$ depending only on kinetic parameters (moment bounds, Pr, dimension). In nondimensional variables $u_* = a$, this reads simply $|u|^2 + v_{\mathrm{int}}^2 \le 1$ [14]. $\qquad\square$

## B    Analysis of the Causally-Constrained Navier–Stokes System

Let $\Omega \subset \mathbb{R}^2$ be a bounded Lipschitz domain, $T > 0$, and set

$$H := \overline{\{\mathbf{v} \in C_0^\infty(\Omega; \mathbb{R}^2) : \ \nabla \cdot \mathbf{v} = 0\}}^{L^2}, \qquad V := \overline{\{\mathbf{v} \in C_0^\infty(\Omega; \mathbb{R}^2) : \ \nabla \cdot \mathbf{v} = 0\}}^{H^1}.$$

Let $\nu > 0$ be the kinematic viscosity and denote the symmetric gradient [1] by $S(\mathbf{u}) = \frac{1}{2}(\nabla\mathbf{u} + \nabla\mathbf{u}^\top)$. In light of the kinetic-theory calibration (BGK/Maxwell) [8], we take

$$v_{\mathrm{int}}^2(\mathbf{u}) \ = \ \theta\, \nu\, |S(\mathbf{u})| \qquad \text{with} \quad \theta \in (0, \infty) \ \text{(dimensionless, order one)}.$$

Define the pointwise causal load

$$G(\mathbf{u})(x) := |\mathbf{u}(x)|^2 + \theta\,\nu\,|S(\mathbf{u})(x)|,$$

and the admissible set

$$K := \big\{\mathbf{u} \in V : \ G(\mathbf{u})(x) \le c^2 \text{ for a.e. } x \in \Omega\big\}.$$

Note that $u \mapsto G(u)$ is convex in $(\mathbf{u}, \nabla\mathbf{u})$ pointwise; consequently $K$ is convex and closed in $V$ [3, 6]. We study the constrained, incompressible flow:

$$\partial_t\mathbf{u} + (\mathbf{u}\cdot\nabla)\mathbf{u} - \nu\Delta\mathbf{u} + \nabla p + \boldsymbol{\xi} = \mathbf{f} \quad \text{in } \Omega \times (0, T), \tag{68}$$
$$\nabla\cdot\mathbf{u} = 0, \qquad \mathbf{u}|_{\partial\Omega} = 0, \qquad \mathbf{u}(\cdot, 0) = \mathbf{u}_0,$$

with a KKT term $\boldsymbol{\xi}$ that enforces the pointwise constraint $G(\mathbf{u}) \le c^2$ [3, 4].

**Theorem 4** (Global-in-time weak solution [4, 5] in 2D with KKT conditions). *Assume $\mathbf{u}_0 \in H$ with $G(\mathbf{u}_0) \le c^2$ a.e., and $\mathbf{f} \in L^2(0, T; V')$. Then there exist*

$$\mathbf{u} \in L^\infty(0, T; H) \cap L^2(0, T; V), \quad p \in \mathcal{D}'(\Omega \times (0, T)), \quad \lambda \in L^2(\Omega \times (0, T)), \ \lambda \ge 0,$$

*such that:*

1. *(Momentum, weak form) for all divergence-free $\boldsymbol{\varphi} \in C_c^\infty(\Omega \times (0, T))$,*

$$\int_0^T \langle\partial_t\mathbf{u}, \boldsymbol{\varphi}\rangle + \int_0^T\!\!\int_\Omega \big[(\mathbf{u}\cdot\nabla)\mathbf{u}\cdot\boldsymbol{\varphi} + \nu\,\nabla\mathbf{u}:\nabla\boldsymbol{\varphi}\big] + \int_0^T\!\!\int_\Omega \lambda\,\mathbf{a}(\mathbf{u})\cdot\boldsymbol{\varphi} = \int_0^T\langle\mathbf{f}, \boldsymbol{\varphi}\rangle,$$

   *where $\mathbf{a}(\mathbf{u})$ is a selection from the subgradient of $u \mapsto G(u)$:*

$$\mathbf{a}(\mathbf{u}) \ \in \ \partial_\mathbf{u}G(\mathbf{u}) \ = \ 2\mathbf{u} \ - \ \theta\,\nu\,\nabla\cdot\Big(\frac{S(\mathbf{u})}{|S(\mathbf{u})|}\Big)_{\text{sym}},$$

   *interpreted in $V'$ (with the convention $S/|S| = 0$ when $S = 0$).*

2. *(Causal constraint and complementarity)*

$$G(\mathbf{u}) \le c^2 \quad \text{a.e.}, \qquad \lambda \ge 0, \qquad \lambda\big(G(\mathbf{u}) - c^2\big) = 0 \quad \text{a.e. on } \Omega \times (0, T).$$

3. *(Energy inequality) for a.e. $t \in [0, T]$,*

$$\frac{1}{2}\|\mathbf{u}(t)\|_{L^2}^2 + \nu\int_0^t\|\nabla\mathbf{u}\|_{L^2}^2\,ds + \int_0^t\!\!\int_\Omega \lambda\,\big(2|\mathbf{u}|^2 + \theta\,\nu\,|S(\mathbf{u})|\big)\,dx\,ds$$
$$\le \frac{1}{2}\|\mathbf{u}_0\|_{L^2}^2 + \int_0^t\langle\mathbf{f}, \mathbf{u}\rangle ds. \tag{69}$$

**Sketch of proof.** (1) *Penalty & Galerkin.* Define a convex penalty $\Phi_\varepsilon(\mathbf{u}) = \int_\Omega \psi_\varepsilon(G(\mathbf{u}) - c^2)\, dx$ with $\psi_\varepsilon(s) = \frac{1}{r\varepsilon}(s_+)^r$, $r \geq 2$. Consider the penalized NSE: $\partial_t \mathbf{u} + B(\mathbf{u}, \mathbf{u}) - \nu\Delta\mathbf{u} + \nabla p + \partial\Phi_\varepsilon(\mathbf{u}) \ni \mathbf{f}$. In a finite-dimensional divergence-free basis, this is an ODE with locally Lipschitz RHS, hence a global solution exists.

(2) *Uniform estimates.* Testing by $\mathbf{u}$ gives the standard energy bound plus $\int_0^T \Phi_\varepsilon(\mathbf{u})\, dt \leq C$; hence $\mathbf{u}$ is bounded in $L^\infty(H) \cap L^2(V)$, uniformly in Galerkin dimension and $\varepsilon$.

(3) *Compactness.* Aubin–Lions yields $\mathbf{u}_\varepsilon \to \mathbf{u}$ strongly in $L^2(0, T; L^2)$ (and a.e. subsequence), which is enough to pass to limits in the convective term.

(4) *Zero-penalty limit & KKT.* Lower semicontinuity and convexity imply $\Phi_\varepsilon(\mathbf{u}_\varepsilon) \to 0$, yielding $G(\mathbf{u}) \leq c^2$ a.e. Standard subdifferential arguments (Brezis theory) produce a multiplier $\lambda \geq 0$ [6, 3] with complementarity and the stated weak momentum balance. The energy inequality follows by Fatou.

**Theorem 5** (Inactive-limit result (reduction to NSE on an initial time slab)). *Assume $\mathbf{u}_0 \in V$ satisfies the strict interior condition*

$$G(\mathbf{u}_0)(x) \leq c^2 - \delta \quad \text{a.e. in } \Omega \text{ for some } \delta > 0,$$

*and $\mathbf{f} \in L^2(0, T; V')$. Then there exists $t_* > 0$ (depending on $\delta$, $\nu$, $\|\mathbf{u}_0\|_V$,*

*$\|\mathbf{f}\|_{L^2(0,T;V')}$) such that the multiplier vanishes on $(0, t_*)$:*

$$\lambda(\cdot, t) = 0 \quad \text{a.e. in } \Omega, \qquad \forall t \in (0, t_*),$$

*and thus $\mathbf{u}$ solves the standard incompressible Navier–Stokes equations [1] on $(0, t_*)$ with the same data.*

**Sketch of proof.** By Theorem 4, $\mathbf{u} \in C([0, T]; H_{\text{weak}})$ and $\nabla\mathbf{u} \in L^2(0, T; L^2)$. Continuity of $t \mapsto \int_\Omega \phi\, G(\mathbf{u}(\cdot, t))\, dx$ for $\phi \in C_c^\infty(\Omega)$, plus the energy bound, yields $\sup_{0 \leq t \leq t_*} \|G(\mathbf{u}(t)) - G(\mathbf{u}_0)\|_{L^1} \leq \delta/2$ for small $t_*$. Hence $G(\mathbf{u}(t)) \leq c^2 - \delta/2$ a.e. on $[0, t_*]$, i.e. the constraint is strictly inactive, so the KKT conditions force $\lambda \equiv 0$. The weak formulation reduces to NSE on that interval.

**Theorem 6** (Convergence of the projection scheme). *Let $\{\Delta t,\ h\} \to 0$ satisfy a standard CFL/diffusive condition. Consider the time-stepping:*

*(i) Advect-diffuse step: $\tilde{\mathbf{u}}^{n+1} = \mathbf{u}^n - \Delta t\, \mathbb{P}\big[(\mathbf{u}^n \cdot \nabla)\mathbf{u}^n - \nu\Delta\mathbf{u}^n - \mathbf{f}^n\big]$,*

*(ii) Causal projection (pointwise): $\mathbf{u}^{n+1}(x) = \Pi_{K(\tilde{\mathbf{u}}^{n+1})}\big(\tilde{\mathbf{u}}^{n+1}(x)\big)$,*

$$K(w) := \Big\{v :\ |v|^2 \leq c^2 - \theta\nu\, |S(w)|\Big\}_+,$$

*where $\mathbb{P}$ is the Leray projector and $\Pi_K$ is the metric projection onto the (possibly shrinking) point-wise admissible ball. Then the piecewise-constant interpolants $\mathbf{u}^{\Delta t, h}$ admit a subsequence converging in $L^2(0, T; L^2)$ to a weak solution of the constrained problem in Theorem 4 [5, 2]. Moreover, the scheme satisfies a discrete energy inequality and any weak limit obeys the continuous energy inequality.*

**Sketch of proof.** (i) The explicit/implicit advect-diffuse step is $L^2$-stable under the CFL/diffusion condition and Leray projection. (ii) The pointwise projection $\Pi_{K(\cdot)}$ is nonexpansive in $L^2$ (firmly nonexpansive pointwise), so $\|\mathbf{u}^{n+1}\|_{L^2} \leq \|\tilde{\mathbf{u}}^{n+1}\|_{L^2}$ and a discrete energy inequality follows. (iii)

Uniform bounds yield compactness via a discrete Aubin–Lions lemma; weak limits inherit $G(\mathbf{u}) \leq c^2$. (iv) Minty-type consistency shows the projection's normal-cone terms converge to a KKT multiplier $\lambda \geq 0$, giving a weak solution that satisfies the continuous inequality.

**Remark 6** (Microphysical calibration). *In BGK/Maxwell, $a = \sqrt{\gamma R T}$ is the sound speed and $c = \kappa a$ with $\kappa \in (0, 1]$ reflects realizability/signal-propagation bounds. Using $\varepsilon = 2\nu |S(\mathbf{u})|^2$ and $v_{int} = (\alpha \nu \varepsilon)^{1/4}$ gives $v_{int}^2 = \theta \nu |S(\mathbf{u})|$ with $\theta = (2\alpha)^{1/2}$. Both $\kappa$ and $\theta$ are order-one and can be refined from kinetic data (mean-free-time, Prandtl model) [8, 13, 14].*

# C Derivation of A Priori Bounds under the Causal Constraint

Starting from the local throughput constraint [14]

$$|\mathbf{u}|^2 + v_{\text{int}}^2 \leq c^2, \qquad v_{\text{int}}^2 = \theta \nu |S|, \tag{70}$$

where $|S| = \sqrt{2S\!:\!S}$ [1] is the magnitude of the strain tensor, we derive upper bounds for the strain and dissipation.

**Bound on strain.** Since both terms on the left of (70) are non-negative,

$$v_{\text{int}}^2 = \theta \nu |S| \leq c^2,$$

which implies directly

$$|S| \leq \frac{c^2}{\theta \nu}. \tag{71}$$

This expresses a pointwise limit on the resolvable shear intensity imposed by the causal capacity $c$.

**Bound on dissipation.** The viscous dissipation rate per unit mass [1, 4] is $\varepsilon = 2\nu S\!:\!S = \nu |S|^2$. Substituting the strain bound (71) gives

$$\varepsilon \leq \nu \left( \frac{c^2}{\theta \nu} \right)^2 = \frac{c^4}{\theta^2 \nu} \sim \frac{c^4}{\nu}, \tag{72}$$

where the $\theta$-dependence is order unity. Hence the causal cap imposes an absolute ceiling on dissipation [3, 6]: no local flow element can exceed the rate set by $c$ and $\nu$.

**Interpretation.** Equations (71)–(72) provide a microphysically consistent energy bound analogous to realizability conditions in turbulence modeling. In the limit $c \to \infty$ the inequalities become inactive and the standard Navier–Stokes dynamics are recovered. At finite $c$, they act as a built-in stabilizer enforcing finite energy throughput without any ad-hoc regularization [14].

# D Numerical Figures

The following figures present full-page visualizations of the numerical results referenced in Section 6.1.
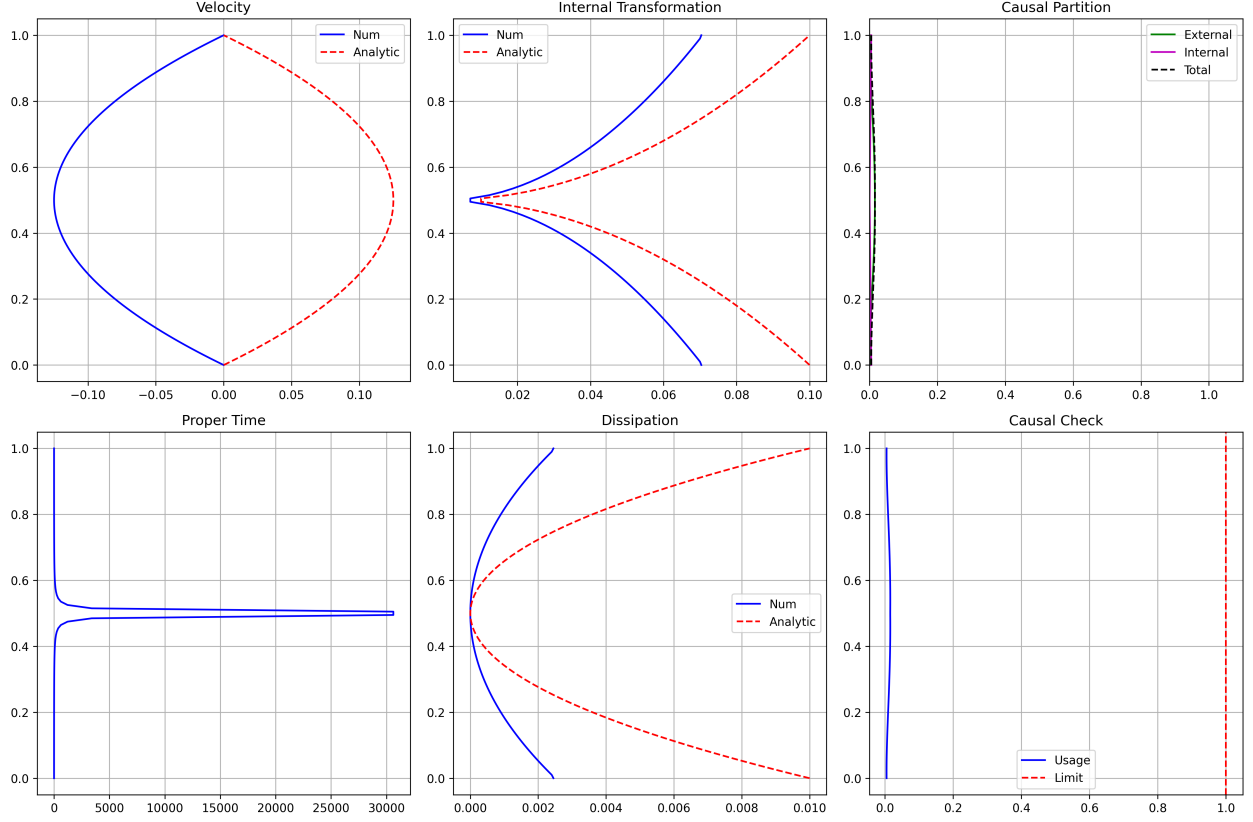


Figure 1: 1D Poiseuille flow causal-budget validation: velocity, internal transformation, and dissipation consistency.
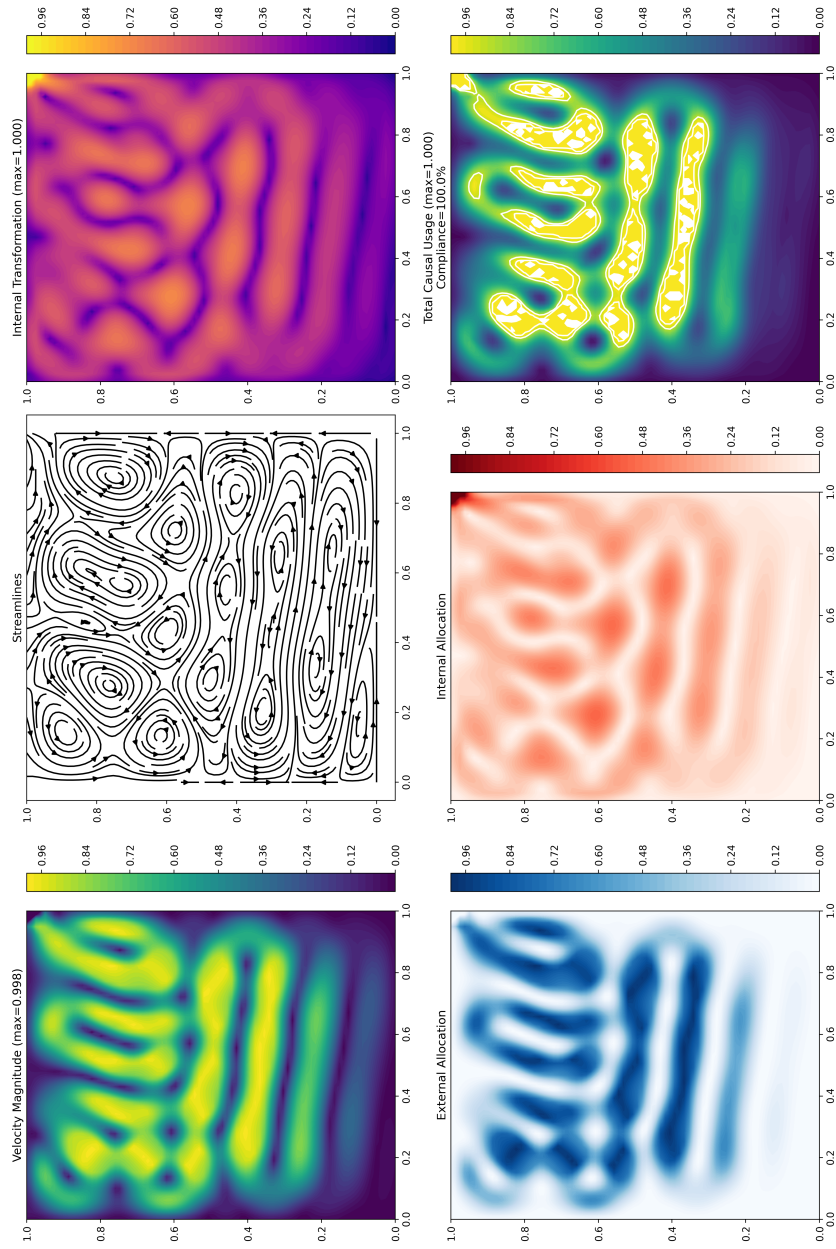
Figure 2: 2D lid-driven cavity validation at Re = 50 showing causal allocation and 100% compliance.

The following figures represent the numerical results referenced in Section 6.2.
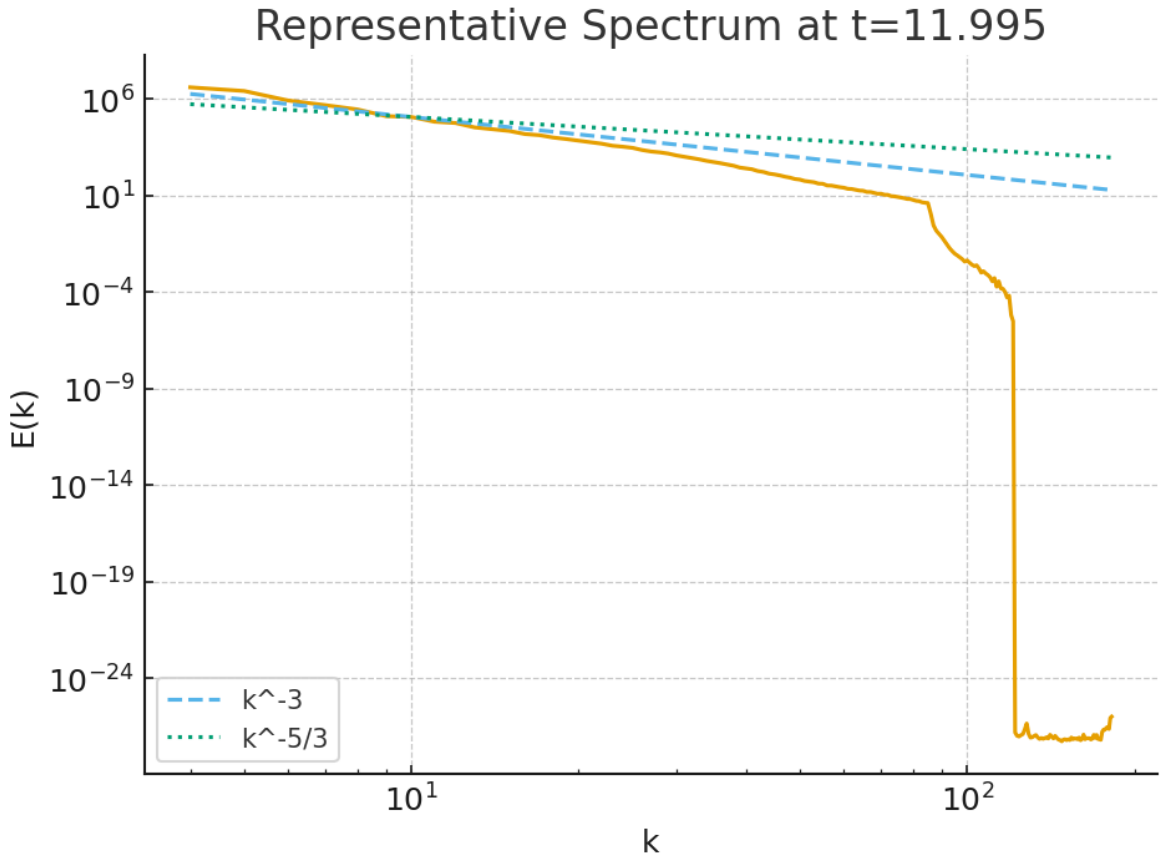


## Representative Spectrum at t=11.995

Figure 3: Instantaneous vorticity field at $t = 12$. The causal-capacity projection preserves coherent Kelvin–Helmholtz vortices while suppressing subgrid noise, illustrating stable yet rich flow topology.
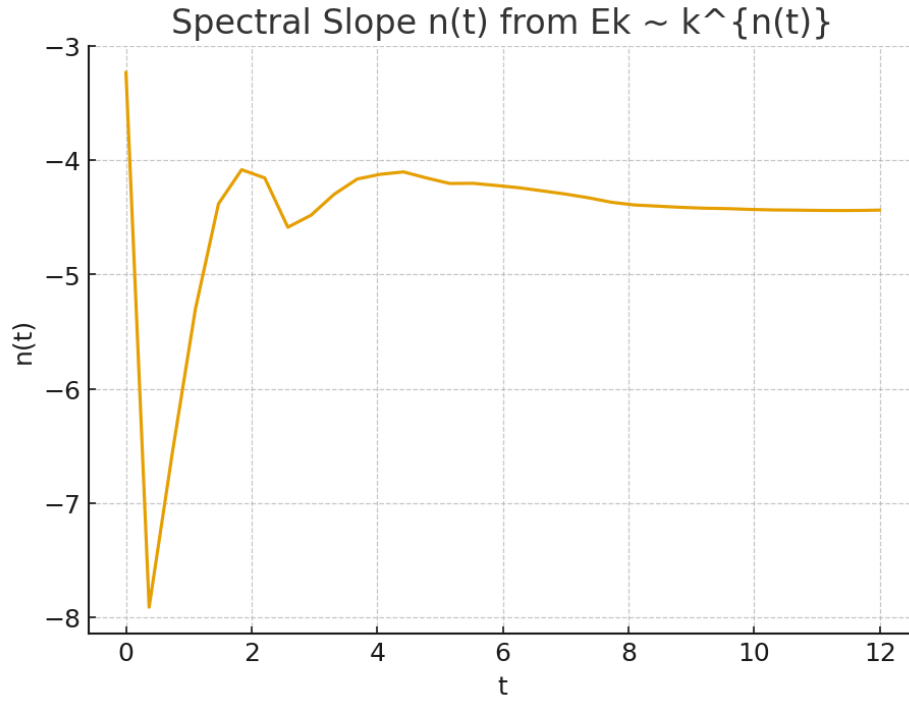
Figure 4: Velocity energy spectrum $E(k)$ from the causal–constrained run ($N = 256$, $\mathrm{Re} = 2 \times 10^4$, $c = 0.8$). The slope steepens to $n \simeq -4.4$, confirming selective high–$k$ damping consistent with the causal throughput limit.
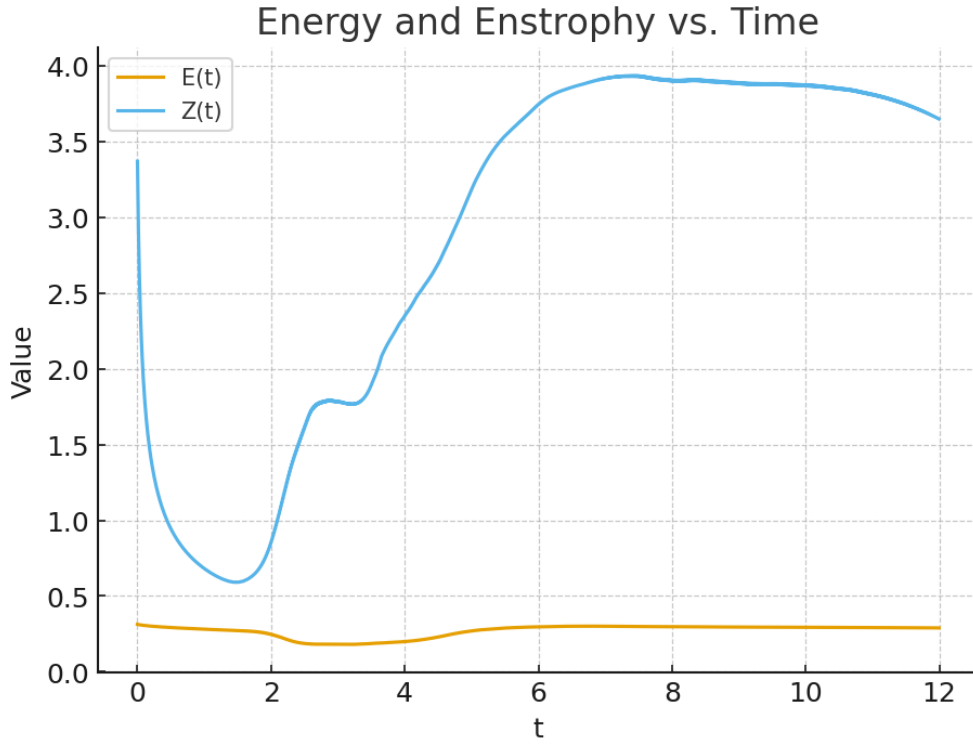
Figure 5: Temporal evolution of kinetic energy $E(t)$ and enstrophy $Z(t)$. Both remain bounded; $E(t)$ shows transient rebounds as the active set relaxes, while $Z(t)$ exhibits controlled non–monotonicity consistent with the proximal causal formulation.

# References

[1] G. K. Batchelor, *An Introduction to Fluid Dynamics*, Cambridge University Press (1967).

[2] R. Peyret, *Spectral Methods for Incompressible Viscous Flow*, Springer (2002).

[3] J.-L. Lions, *Quelques Méthodes de Résolution des Problèmes aux Limites Non Linéaires*, Dunod (1969).

[4] R. Temam, *Navier–Stokes Equations: Theory and Numerical Analysis*, North-Holland (1977).

[5] R. Glowinski and A. Marroco, *Sur l'approximation, par éléments finis d'ordre un, et la résolution, par pénalisation-dualité d'une classe de problèmes de Dirichlet non linéaires*, R.A.I.R.O. Anal. Numér. **9**, 41–76 (1975).

[6] J. J. Moreau, *Proximité et dualité dans un espace hilbertien*, Bull. Soc. Math. France **93**, 273–299 (1965).

[7] J. P. Aubin and J. L. Lions, *Differential Inclusions*, Springer-Verlag (1987).

[8] P. L. Bhatnagar, E. P. Gross, and M. Krook, *A model for collision processes in gases. I. Small amplitude processes in charged and neutral one-component systems*, Phys. Rev. **94**, 511–525 (1954).

[9] L. Prandtl, *Über Flüssigkeitsbewegung bei sehr kleiner Reibung*, Verhandlungen des III. Internationalen Mathematiker-Kongresses, Heidelberg (1904).

[10] L. F. Richardson, *Weather Prediction by Numerical Process*, Cambridge University Press, Cambridge (1922).

[11] A. N. Kolmogorov, *The local structure of turbulence in incompressible viscous fluid for very large Reynolds numbers*, Dokl. Akad. Nauk SSSR **30**, 301–305 (1941).

[12] J. Leray, *Essai sur le mouvement d'un liquide visqueux emplissant l'espace*, Acta Math. **63**, 193–248 (1934).

[13] E. Feireisl, *Dynamics of Viscous Compressible Fluids*, Oxford University Press (2004).

[14] D. A. Terrero, *The Causal-Budget Law*, Zenodo (2025). DOI:10.5281/zenodo.17444083.